Anal. Chem. **2007,** *79,* 3810−3820

Characterization and Optimization of Gold Nanoparticle-Based Silver-Enhanced Immunoassays

Shalini Gupta, Sabil Huda, Peter K. Kilpatrick, and Orlin D. Velev*

Department of Chemical and Biomolecular Engineering, North Carolina State University, Raleigh, North Carolina 27695-7905

Silver-enhanced nanoparticle-labeled immunoassays provide a simple, low-cost, and effective way of detecting antigens in dilute solutions. The physical mechanisms behind their operation, however, have not been fully investigated. We present a semiquantitative approach for optimizing sandwich nanoparticle immunoassays using an adsorption-controlled kinetic model. Primary antibodies were immobilized on a solid substrate to bind the target antigens in solution. An optical signal was measured by secondary labeling of antigens with gold nanoparticles and their enhancement by silver nucleation. The opacity of the silver-enhanced spots was quantified by densitometry. The selectivity of the sandwich immunoassays was adequately high, and antigen concentrations as low as 0.1 μg cm^{-3} (4 ng total) were detected reproducibly. The role of mass transfer was investigated, and a model was developed to optimize the performance of immunoassays by correlating the opacities of silver spots to the concentration and incubation times of antigens and gold nanoparticles. The results could allow the development of more rapid and reliable nanoparticle immunoassays.

Diagnostic immunoassays are routinely used for biomolecular detection because they are simple, sensitive, and allow parallelization. Antigens such as proteins, antibodies, viruses, drugs, and other molecules, generally referred to as the analyte in an immunoassay, are selectively bound by their complementary immunoglobulins either in solution (agglutination assay) or on a solid surface (direct or sandwich assay). The bound antigens are detected with a reporter, typically an antibody that is labeled with a probe, and the intensity of the signal corresponding to the number of antigen−antibody complexes formed is measured.[1,2]

The immunoassay formats differ in the type of probe and signal amplification techniques that are used in the detection process. Enzyme-linked immunosorbent assay (ELISA) is one of the oldest (ca. 1960) and most widely used laboratory method. It yields a colorimetric signal upon enzymatic cleavage of chemiluminescent substrate[3−5] and has limits of detection in the picomolar analyte range. Fluorescence immunoassays, which are frequently used in cell biology, are based on an alternative detection strategy where antibodies labeled with fluorophores (Rhodamine, Alexa fluor, FITC, etc.) are used as markers that provide high optical contrast and do not require an additional processing step.[6,7] Extra care is, however, needed to avoid photobleaching of the fluorophores, which may lead to reduced accuracy. Both ELISA and fluorescence immunoassays are routinely performed in a microarray format for higher throughput and greater selectivity. A few alternative immunoassay techniques make use of immunochromatography,[8,9] gel electrophoresis,[10] radioisotope (^{125}I, ^{3}H) labeling,[5,11] electrochemical sensing,[12] scanometry,[13] and surface-enhanced Raman spectroscopy.[14,15]

Latex agglutination tests (LATs) have been used since the late 1950s. In LATs, antibody-coated microspheres are agglutinated and precipitated from suspension in the presence of antigens. LATs have contributed greatly to diagnostic immunology because they are inexpensive, portable, and yield results rapidly. The detection is typically carried out by light scattering or by visual inspection.[16] One popular modification of LATs is the strip tests where the agglutination event is made visible by the colored bands of antibody-conjugated particles bound by the antigen to the surface. More recent advances have been made using nanoparticles as detection probes, because their nanometer size gives rise to high diffusion coefficients and their optoelectrical properties can be tailored chemically or physically and used in the detection procedures.[17] The nanoparticle-based surface immunoassays require only a few microliters of the sample and may be miniaturized.[18−20]

* Corresponding author: (phone) (919) 513-4318; (fax) (919) 515-3465; (e-mail) odvelev@unity.ncsu.edu.

(1) Morgan, C. L.; Newman, D. J.; Price, C. P. *Clin. Chem.* **1996**, *42*, 193−209.
(2) Andreotti, P. E.; Ludwig, G. V.; Peruski, A. H.; Tuite, J. J.; Morse, S. S.; Peruski, L. F. *Biotechniques* **2003**, *35*, 850−859.
(3) Engvall, E.; Perlman, P. *Immunochemistry* **2003**, *8*, 871−874.
(4) Mendoza, L. G.; McQuary, P.; Mongan, A.; Gangadharan, R.; Brignac, S.; Eggers, M. *BioTechniques* **1999**, *27*, 778−788.
(5) Goldberg, M. E.; Djavadi-Ohaniance, L. *Curr. Opin. Immunol.* **1993**, *5*, 278−281.
(6) Macbeath, G.; Schreiber, S. L. *Science* **2000**, *289*, 1760−1763.
(7) Stephens, D. J.; Allan, V. J. *Science* **2003**, *300*, 82−86.
(8) Weller, M. G. *Fresenius J. Anal. Chem.* **2000**, *366*, 635−645.
(9) Shyu, R. H.; Shyu, H. F.; Liu, H. W.; Tang, S. S. *Toxicon* **2002**, *40*, 255−258.
(10) Goldenberg, D. P.; Creighton, T. E. *Anal. Biochem.* **1984**, *138*, 1−18.
(11) Shan, G.; Huang, W.; Gee, S. J.; Buchholz, B. A.; Vogel, J. S.; Hammock, B. D. *Proc. Natl. Acad. Sci. U.S.A.* **2000**, *97*, 2445−2449.
(12) Lee, T. M.; Li, L.; Hsing, I. *Langmuir* **2003**, *19*, 4338−4343.
(13) Taton, T. A.; Mirkin, C. A.; Letsinger, R. L. *Science* **2000**, *289*, 1757−1760.
(14) Xu, W.; Xu, S.; Ji, X.; Song, B.; Yuan, H.; Ma, L.; Bai, Y. *Colloids Surf., B* **2005**, *40*, 169−172.
(15) Cao, Y. C.; Jin, R.; Mirkin, C. A. *Science* **2002**, *297*, 1536−1540.
(16) Bangs, L. B. *Pure Appl. Chem.* **1996**, *68*, 1873−1879.
(17) Kawaguchi, H. *Prog. Polym. Sci.* **2000**, *25*, 1171−1210.
(18) Kusnezow, W.; Hoheisel, J. D. *J. Mol. Recognit.* **2003**, *16*, 165−176.

10.1021/ac062341m CCC: $37.00 © 2007 American Chemical Society
Published on Web 04/13/2007

Detection based on the nanoparticle color may not be sensitive enough due to the tiny amount of material present unless the particles are in proximity.[21] The sensitivity and ease of detection in the case of gold or silver nanoparticle probes can be increased drastically by using "silver enhancement",[22−24] a procedure for electroless silver deposition where the nanoparticles act as nuclei. In this technique, colloidal metal particles act as catalysts to reduce silver ions (I) to metallic silver in the presence of a reducing agent (such as hydroquinone) and are enlarged in the process by up to 5 orders of magnitude. The amount of metallic silver deposited is typically quantified by electrochemical measurements,[25] anodic stripping analysis,[26] or colorimetry[27,28] among other methods. A few examples of immunoassays using colloidal gold nanoparticles combined with silver enhancement have been demonstrated on microarrayed substrates,[29] between coplanar electrodes,[30−32] and through microfluidic channels.[33]

The nanoparticle immunoassay techniques and especially the complex sandwich assays are poorly characterized in terms of the relation between mass transfer and performance. For example, the incubation time required for the saturation of the receptor sites with antigens or nanoparticle labels is commonly established either empirically or by operator judgment. Antibodies conjugated to gold nanoparticles are typically incubated for a longer period of time than molecular antigens owing to their larger size. Good understanding of the fundamentals of mass transfer is required to optimize the overall performance of a nanoparticle sandwich immunoassay.[34,35]

In this paper, we report the use of silver enhancement as a semiquantitative means of determining the concentration of gold nanoparticles on a surface. We also illustrate that the optically measured darkness of the enhanced spots could be a simple tool to compare and characterize the rate of mass transfer of antigens and gold nanoparticles in the system. The aim of our work is to (i) provide a simple procedure to assemble a compact, rapid, and low-cost sandwich immunoassay using a combination of gold nanoparticle labels and silver amplification technique, (ii) investigate to what extent the nanoparticle adsorption can be quantified using silver enhancement, (iii) characterize the immunoassay's selectivity and sensitivity via optical densitometry, (iv) match the adsorption kinetics against a simple mass-transfer model, and (v) formulate on the basis of the analysis a general procedure for optimizing the operation time of the assay by studying the adsorption kinetics of each reagent individually.

Kinetics of Analyte Adsorption. We used a simple unified model for the adsorption kinetics of the species onto the binding sites on the surface. During the adsorption process in surface immunoassays, the antigen molecules in the buffer freely diffuse toward the solid substrate (semi-infinite diffusion to a plane), where they may either attach with high affinity to the binding sites on the antibodies or adsorb nonspecifically to the surface. At steady state, assuming negligible convection in the very thin chamber used, the relation between the rate of change of surface coverage by an adsorbing species and the concentration gradient adjacent to the surface follows from a simple mass balance at the surface[36]

$$\mathrm{d}\Gamma/\mathrm{d}t = D(\partial c/\partial x)_{x=0} \tag{1}$$

In the above expression, D is the diffusion coefficient ($cm^2\ s^{-1}$) and Γ is the surface coverage (molecules cm^{-2}). The kinetic eq 1 may be related to the rate of diffusion in solution (J_D) or to a simple Langmuir-type first-order rate of adsorption (for low coverage) at the surface (J_R),

$$J_D = D(c_b - c_s)/L \tag{2}$$

$$J_R = k_{ads}c_s(\Gamma_{max} - \Gamma) \tag{3}$$

where c_b is the bulk concentration of the adsorbing species (molecules cm^{-3}), c_s is the concentration of the adsorbing species in the vicinity of the surface, L is the diffusion path length (cm), k_{ads} is the adsorption rate constant (cm^3 molecules^{-1} s^{-1}), and Γ_{max} is the total number of free sites available per unit surface area. At steady state, $J_D = J_R$ and a simple relation follows from eqs 2 and 3,

$$c_s = \frac{c_b}{1 + k_{ads}L(\Gamma_{max} - \Gamma)/D} = \frac{c_b}{1 + \Theta} \tag{4}$$

Here, the dimensionless parameter $\Theta = k_{ads}L(\Gamma_{max} - \Gamma)/D$ is known as the Thiele modulus.[36] For $\Theta \gg 1$, c_s approaches zero. In other words, as soon as a diffusing molecule reaches the surface it is adsorbed and the rate of surface coverage is determined by the rate of diffusion in solution ($J_D = Dc_b/L$). For $\Theta \ll 1$, c_s approaches the bulk concentration (c_b); i.e., the diffusion in the solution is much faster than adsorption and the kinetics of the process is governed by the rate of adsorption at the surface, $J_R = k_{ads}c_b(\Gamma_{max} - \Gamma)$. In all other nonlimiting cases, a numerical procedure can be used to determine the concentration gradient at the surface.

MATERIALS AND METHODS

Immunoassay Principles. The main steps of the immunoassay that we developed are schematically outlined in Figure 1. The

(19) Angenendt, P. *Drug Discovery Today* **2005**, *10*, 503−511.
(20) Nielson, U. B.; Geierstanger, B. H. *J. Immunol. Methods* **2004**, *290*, 107−120.
(21) Thaxton, C. S.; Mirkin, C. A. *Nat. Biotechnol.* **2005**, *23*, 681−682.
(22) Lackie, P. M. *Histochem. Cell. Biol.* **1996**, *106*, 9−17.
(23) Stierhof, Y.-D.; Humbel, B. M.; Schwarz, H. *J. Electron Microsc. Technol.* **1991**, *17*, 336−343.
(24) Baschong, W.; Stierhof, Y.-D. *Microsc. Res. Technol.* **1998**, *42*, 66−79.
(25) Cai, H.; Wang, Y.; He, P.; Fang, Y. *Anal. Chim. Acta* **2002**, *469*, 165−172.
(26) Chu, X.; Fu, X.; Chen, K.; Shen, G.-L.; Yu, R.-Q. *Biosens. Bioelectron.* **2005**, *20*, 1805−1812.
(27) Guo, H. S.; Yang, D.; Gu, C. R.; Bian, Z. P.; He, N. Y.; Zhang, J. N. *J Nanosci. Nanotechnol.* **2005**, *5*, 2161−2166.
(28) Alexandre, I.; Hamels, S.; Dufour, S.; Collet, J.; Zammatteo, N.; De Longueville, F.; Gala, J.-L.; Remacle, J. *Anal. Biochem.* **2001**, *295*, 1−8.
(29) Liang, R.-Q.; Tan, C.-Y.; Ruan, K.-C. *J. Immunol. Methods* **2004**, *285*, 157−163.
(30) Velev, O. D.; Kaler, E. W. *Langmuir* **1999**, *15*, 3693−3698.
(31) Moller, R.; Csaki, A.; Kohler, J. M.; Fritzsche, W. *Langmuir* **2001**, *17*, 5426−5430.
(32) Park, S.-J.; Taton, T. A.; Mirkin, C. A. *Science* **2002**, *295*, 1503−1506.
(33) Sia, S. K.; Linder, V.; Parviz, B. A.; Siegel, A.; Whitesides, G. M. *Angew. Chem., Int. Ed.* **2004**, *43*, 498−502.
(34) Zimmermann, M.; Delamarche, E.; Wolf, M.; Hunziker, P. *Biomed. Microdevices* **2005**, *7*, 99−110.
(35) Merrill, S. J. *J. Immunol. Methods* **1998**, *216*, 69−92.
(36) Fogler, H. S. *Elements of Chemical Reaction Engineering*; Prentice Hall of India Private Ltd: New Delhi, India, 2001.

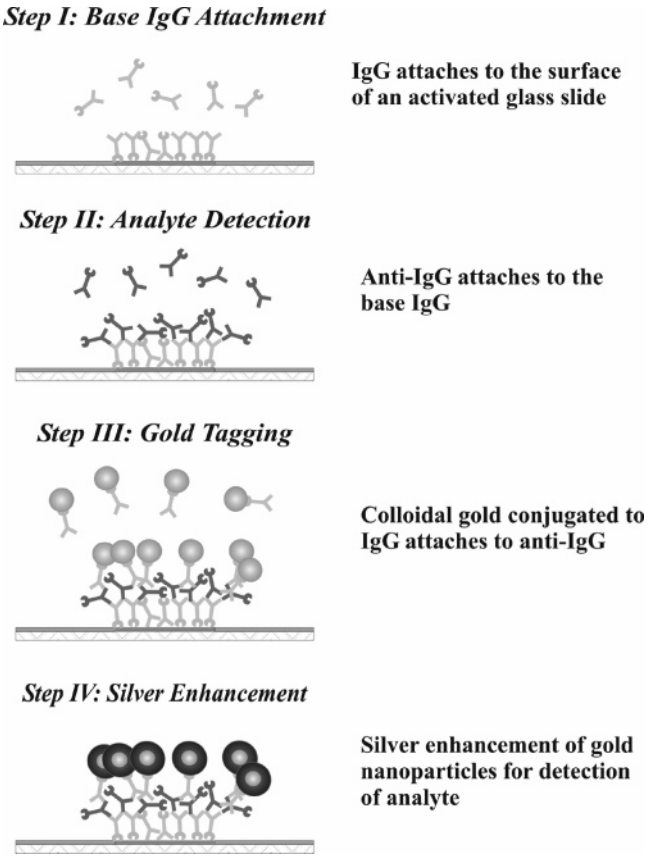

Figure 1. Schematic of the sandwich immunoassay depicting the sequential steps followed during the experiment. The figure is not drawn to scale.

assay was performed on microscope glass slides, which were activated with aldehyde-terminated silanes using standard coupling chemistry. The silane ends of the molecules attach to the glass substrate leaving the aldehyde groups available to react with amine groups on the proteins. Primary antibodies were irreversibly attached to the aldehydes on the substrate via formation of Schiff's base links (step I). The glass slide was washed off to remove any unbound antibodies, and the unreacted aldehydes were reacted with bovine serum albumin (BSA), which was used as a blocking agent to prevent nonspecific adsorption of the antigens in the next step. BSA and nonionic surfactant (Tween-20) were also added to the antigen and nanoparticle solutions to minimize nonspecific binding and aggregation.

A few microliters of dilute antigen solution were incubated over the glass substrate to allow the binding of antigens to the primary antibodies in the immobilized spot (step II). Unbound antigens were removed from the glass slide by washing with a mixture of BSA and surfactant. The bound antigens were sequentially tagged with gold nanoparticles by incubating the assay chamber with a dilute suspension of secondary antibodies conjugated to colloidal gold (step III). The attached gold nanoparticles were enlarged by silver metal deposition (step IV). Silver enhancement proceeds as an autocatalytic reaction: the gold nanoparticles serve as nucleation sites to catalyze the reduction of silver ions to metallic silver. The enhanced plates were washed, dried, and characterized by microscopy and optical densitometry.

Antibodies and Reagents. The following immunoglobulins (IgGs) were used in the experiments: monoclonal goat anti-mouse (GAM IgG) and goat anti-rabbit (GAR IgG) antibodies (Jackson ImmunoResearch Lab Inc.; West Grove, PA); mouse (M IgG) and rabbit (R IgG) antibodies acting as their antigens (Calbiochem; San Diego, CA); 5-nm colloidal gold conjugated to goat anti-mouse (GAMg IgG) and goat anti-rabbit (GARg IgG) antibodies (Ted Pella, Inc.; Redding, CA). Other reagents used include the following: 11-(triethoxysilyl)undecanaldehyde (Gelest, Inc.; Morrisville, PA); phosphate buffer saline, BSA, ≥99% acetone, (3-aminopropyl)triethoxysilane (APTES), and anhydrous toluene (Sigma; St. Louis, MO); Tween-20 and light microscopy silver enhancement kit (Ted Pella, Inc.). All reagents were used as received.

Substrate Preparation and Experimental Setup. Microscope glass slides (Fisher Scientific, PA) were immersed in a strong oxidizing solution (Nochromix) overnight, washed with deionized (DI) Millipore water (resistivity ~18 MΩ cm), and oven-dried for ~1 h. A 2% solution of 11-(triethoxysilyl)undecanaldehyde was freshly prepared in dry acetone and a 10-μL droplet of it was placed on the clean glass slides for 5 min. The silane reagent was rinsed off using DI water, and the slide was air-dried.

The immunoassay was performed in a transparent 18-μL flow cell (HBW13, Grace BioLabs; Bend, OR) as shown in Figure 2a. The cell contained two openings through one of which the reagents were manually injected using a micropipet and through the other withdrawn controllably using a micropump. Importantly, the Teflon tubing connected to the withdrawal pump was of diameter smaller than the cell opening into which it was inserted. This allowed for the level of the liquid in the chamber to be maintained even though the pump could be kept running continuously. When new liquid was added through the inlet opening, it replaced the contents of the microchamber by laminar flow and was sucked by the end of the tubing connected to the pump. After the excess liquid in the cell was sucked in the tubing, however, the capillary meniscus between the end of the tube and the opening of the cell broke, leaving the cell full of liquid. Thus, the contents of the cell were rapidly and easily displaced at the end of each step of the protocol without ever exposing the functionalized surface to air.

Immunoassay Protocol. The samples containing IgGs, BSA, and Tween-20 were prepared in 10 mM phosphate buffer saline (PBS) at pH 7.4. The range of concentrations of reagents and the incubation times used in the experimental steps are listed in Table 1. All experiments were performed at room temperature.

The assay was initiated when 0.2 μL of buffer containing 50 μg cm^{-3} GAM IgG was carefully placed on the aldehyde-functionalized glass slide for 5 min and sealed with the flow chamber. Drying of the solution was minimized to avoid denaturation of the IgGs on the substrate. The chamber was then filled and incubated for 15 min with BSA followed by 15-min incubation with a mixture of BSA and Tween-20. The contents of the chamber were replaced with varying concentrations of M IgG (antigen) and incubated for different periods of time (ranges shown in Table 1). This step was followed by 10-min incubation with the BSA and Tween-20 mixture. Dilute suspensions of GAMg IgGs (nanoparticle labels) were incubated in the chamber for varying periods of time. The excess colloidal gold was washed off with the BSA and Tween-20 mixture. The chamber was rinsed thoroughly with DI Millipore water. The washing step was essential to remove all

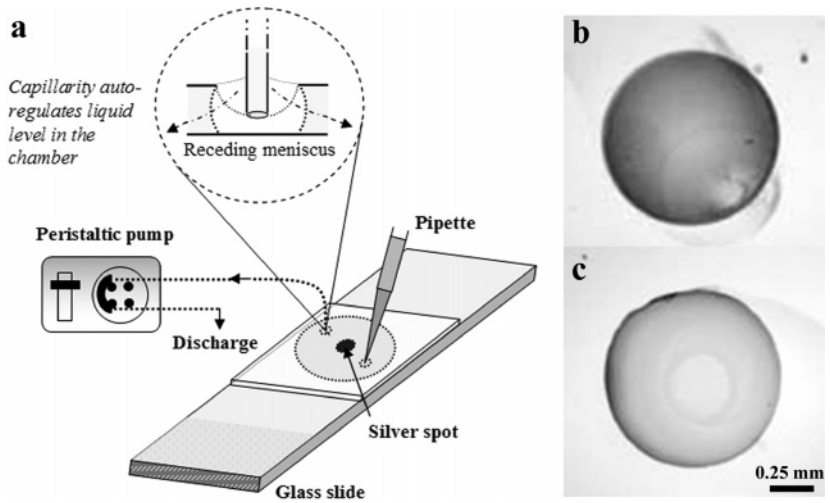

Figure 2. (a) Experimental setup for performing the immunoassay. (b, c) Examples of two silver-enhanced spots. The spot in (b) was obtained with a mouse IgG concentration of 30 μg cm^{-3} incubated for 30 min with gold nanoparticle suspension, and (c) was obtained with a mouse IgG concentration of 1 μg cm^{-3} incubated for 45 min with gold nanoparticle suspension. All other conditions were maintained constant.

Table 1. Range of Concentrations and Incubation Times of All Solutions Used in Developing the Immunoassays[a]

type of solution	concentration	time of incubation (min)
goat anti-mouse IgG	50 μg cm^{-3}	5
BSA	0.3 wt %	15
BSA and Tween-20 mixture	0.15 wt % (BSA) and 0.25 wt % (Tween-20)	10 and 15
mouse IgG	1−50 μg cm^{-3}	0.2−80
goat anti-mouse IgG conjugated gold nanoparticles	2×10^{11}−9×10^{13} particles cm^{-3}	0.5−300
silver initiator and enhancer	1:1 vol %	10

[a] All solutions except the ones for silver enhancement were prepared in 10 mM PBS at pH 7.4.

free ions, which could result in background noise in the consecutive enhancement step. The gold nanoparticles were silver enhanced for 10 min with a mixture of equal volumes of the initiator and enhancer provided in the light microscopy silver enhancement kit. The silver-enhanced spot was washed extensively with DI water to remove the unreacted silver ions. The opacity of the spot was quantified (after air-drying) by densitometry analysis. Each experiment was repeated twice before data analysis.

Optical Densitometry Analysis. The silver-enhanced spots were viewed in transmitted light mode using an Olympus BX61 optical microscope. The dark black (or brown) silver deposit had good contrast against the transparent glass background. Typical optical images of ~1-mm-sized silver-labeled spots are shown in Figure 2b and c. The images were captured in gray scale (8 bits/channel) at a fixed exposure time of 1/1200 s using an Olympus DP70 CCD digital camera. The total area of the silver-enhanced spot in each image was selected using the lasso tool in the Adobe Photoshop software (version 7.0.1). The darkness (I_S) of each spot was quantified by measuring its average opacity using the luminosity histogram tool in Photoshop. The data were normalized by the opacity of the background (I_b), which was calculated by selecting a clean area from the sector surrounding the spot. The normalization procedure was necessary to correct for the background scattering, which could vary slightly from one experiment to another. The final signal was recorded as an "optical darkness ratio" (ODR) of the relative intensities of the enhanced spot (I_S) and the background (I_b)

$$\mathrm{ODR} = (I_b - I_s)/I_b \quad (5)$$

The final ODR value was plotted as an average of the two data points obtained by repeating each experiment. The ODR values of the two data points were indicated as error bars. Please note that ODR is different from the spectroscopic optical density, which is defined as a logarithm of the corresponding intensity.

Formation of Gold Gradients via APTES Monolayer Self-Assembly. In order to characterize the silver-enhancing procedure, a cycle of silver enhancement experiments were performed with gold nanoparticles deposited in a gradient of changing surface concentration. The procedures used in making and studying well-defined nanoparticle gradient substrates are as follows.

(i) Substrate Treatment. A microscope glass slide was cut into 7.5 cm × 1.25 cm rectangular pieces and dipped in Nochromix overnight. The slide was washed thoroughly with DI water prior to the experiment and air-dried. It was then cleaned and hydrophilized by ultraviolet/ozone (UVO) treatment for 30 min.

(ii) APTES Monolayer Self-Assembly. A 1 wt % solution of APTES was prepared in anhydrous toluene and enclosed in a container. The solution was heated to 60 °C in a water bath, and the UVO-treated glass slide was immersed in it. The slide was taken out of the container after 6 min and immediately dipped into toluene. The slide was sonicated in toluene and ethanol for 5 min each to remove the physiosorbed silane molecules, washed with DI water, and completely dried in air.

(iii) Deposition of Gold Nanoparticle Gradients. An aqueous suspension of ~12-nm gold particles was synthesized by citrate reduction of $HAuCl_4$ (ACS reagent, Aldrich; St. Louis, MO).[37,38] One end (~1 cm) of the APTES-coated substrate was

(37) Slot, J. W.; Geuze, H. J. *Eur. J. Cell Biol.* **1985**, *38*, 87−93.

Table 2. Selectivity Control Table[a]

immunoglobulins on the surface		immunoglobulins incubated in the solution					
		GAMg	GARg	M + GAMg	M + GARg	R + GAMg	R + GARg
direct assays	M	√	×	√	x	√	×
	R	√(FP)	√	√(FP)	√	√(FP)	√
sandwich assays	GAM	×	×	√	×	×	×
	GAR	×	×	×	×	×	√

[a] The symbols represent enhancement (√), no enhancement (×), and false positive (√(FP)).

dipped in the gold suspension for 2−3 h to ensure complete saturation of nanoparticles on the surface. The chamber was then slowly filled with the gold suspension at a rate of ~0.83 mm min^{-1} until the other end of the substrate was also completely submerged in the colloidal solution. The varying exposure time lead to decreasing Au nanoparticle adsorption along the height of the substrate. The substrate was withdrawn from the gold suspension, washed with DI water, and air-dried.

(iv) Surface Characterization. To determine the number density of gold nanoparticles, 1 μm × 1 μm tapping mode scans were taken with a digital Nanoscope IIIa controller atomic force microscope (AFM; Veeco; Santa Barbara, CA) at various positions on the substrate along the direction of the gradient (*x*-dir). The particle densities were obtained by manually counting the particles in the AFM micrographs. The results were averaged by taking two transverse measurements (in the *y*-dir) for each position.

The gradient substrates were silver enhanced for 10 min following the standard procedure, washed with DI water, and air-dried. The slides were imaged in the optical microscope at the same positions as the previous AFM measurements. We also scratched off a portion of silver at these positions to obtain ~1-mm silver islands similar in shape to the typical immunoassay spots (Figure 2b and c). These spots were also imaged in the optical microscope. All images were analyzed by densitometry with the same microscope and camera settings as for the immunoassay experiments. We obtained similar results in both cases, which indicated that the densitometry method is independent of the spot size and that there is little effect of scattering from the edges of the silver deposits. The topography of gold nanoparticles, before and after silver enhancement, was characterized using a JEOL 6400F field emission scanning electron microscope.

RESULTS AND DISCUSSION

Assay Selectivity. Our initial experiments evaluated the selectivity of the assay in distinguishing two types of polyclonal immunoglobulins. Antigens may bind nonspecifically (via hydrophobic or electrostatic interactions) to the substrate surface or to the immobilized antibodies to yield false positive results. On the other hand, specific binding of the antigens or the nanoparticle labels may be too weak due to surface hindrance or immunoglobulin degradation, leading to false negative results. These false positives or false negatives must be minimized for accurate detection. Thus, the first series of experiments were aimed to demonstrate the viability of our immunoassay and to gauge its selectivity. Four types of immunoglobulins were used, namely, goat anti-mouse, mouse, goat anti-rabbit, and rabbit IgGs. Direct and sandwich assays were performed using the standard experimental procedures.

In direct assays, antigens (M and R IgGs) were immobilized on an aldehyde-functionalized glass surface and incubated with antibody-conjugated gold nanoparticles (GAMg and GARg IgGs) in solution. This is not a practical assay, but it allows estimating the selectivity of each single binding event. Immobilized antigens were also incubated first with antigens (M and R IgGs) in solution and then with antibody nanoparticle conjugates. This first incubation step is of little practical value because the final binding events occur directly between the immunoglobulins on the surface and the ones on the gold nanoparticles (without any role of the intermediate immunoglobulin), but it allows estimating the impact of nonselective binding events taking place in the system. In the realistic sandwich assays, primary antibodies (GAM and GAR IgGs) were immobilized on the aldehyde-functionalized glass and the remaining steps were as shown in Figure 1. The outcomes of all possible combinations in the cross-reactivity experiments are presented in Table 2.

No false negatives were recorded in any experiment. All of the sandwich assays performed as expected and were selective to the type of immunoglobulin. Three false positive results were, however, observed in direct assays, which seem to have been a result of nonspecific interaction between R IgG and GAMg IgG. The lack of false positives in the sandwich assays probably results from the two-step process where R IgG binds first with GAM IgGs immobilized on the surface and second with GAMg IgGs in solution. The probability of two nonselective binding events occurring for a particular antigen is expected to be much smaller compared to a single attachment step in direct assays.[18,19] If necessary, nonspecific binding can be further reduced by increasing the number of washing steps, using higher concentrations of BSA and Tween-20, adjusting the pH, adding glycerol (to reduce hydrophobic interactions), increasing the salt concentration (up to 500 mM NaCl), and binding of the antibodies to the surface in an oriented fashion to minimize heterogeneities;[39,40] however, that was not necessary for the sandwich format. Having proven that the actual sandwich immunoassays yield accurate results, we proceeded with the sandwich configuration in all of the following immunoassay experiments.

Estimation of Thiele Modulus for the Kinetic Model Based on the System Parameters. To identify the limiting kinetics of

(38) Hayat, M. A. *Colloidal Gold: Principles, Methods, and Applications*; Academic Press, Inc.: San Diego, CA, 1991; Vol. 3.

(39) Lu, B.; Smyth, M. R.; O'Kennedy, R. *Analyst* **1996**, *121*, 29R−32R.

(40) Vijayendran, R. A.; Leckband, D. E. *Anal. Chem.* **2001**, *73*, 471−480.

our process, we estimated the Thiele modulus based on the known assay parameters. The random sequential adsorption model for monodispersed charged spheres predicts that the jamming limit beyond which no more antibody-conjugated gold nanoparticles can be placed on a homogeneous surface is $\sim 5 \times 10^{11}$ particles cm^{-2}.[41] Previous studies have also shown that the specific binding capacity of randomly oriented antibodies covalently attached to a solid substrate is ~ 25 ng cm^{-2}.[40,42] This yields an antigen packing density of $\sim 10^{11}$ molecules cm^{-2}. In our sandwich assays, the antigens are further bound by secondary antibodies conjugated to bulky gold nanoparticles. The surface density of gold nanoparticles is therefore expected to be lower (by almost 1 order of magnitude) than the concentration of antigens on the surface. We used $\Gamma_{max} = 10^{10}$ gold nanoparticles cm^{-2} for our Thiele modulus calculations. This value corresponds to the maximal particle surface density estimated by comparing the nanoparticle gradient and real assay experiments described in the next section.

The value of the diffusion coefficient, $D = 5 \times 10^{-7}$ cm^2 s^{-1}, was estimated using the Stokes−Einstein equation ($D = k_B T/6\pi\eta r$). The height of the flow cell was $L = 0.015$ cm. The order of magnitude of the adsorption rate constant, $k_{ads} \cong 10^{-16}$ cm^3 $molecules^{-1}$ s^{-1}, was estimated based on values reported in the literature.[34,40,43,44] Based on the above parameter values, Thiele modulus was estimated to be $\ll 1$ and eq 1 reduced to a simple adsorption-controlled kinetic relation[36]

$$d\Gamma/dt = k_{ads} c_b (\Gamma_{max} - \Gamma) \qquad (6)$$

All experiments were conducted at constant temperature so k_{ads} remains constant. Equation 6 can be analytically integrated using the initial condition $\Gamma(0) = 0$ to give the coverage with time,

$$\Gamma/\Gamma_{max} = 1 - \exp(-k_{ads} c_b t) \qquad (7)$$

As will become clear in the forthcoming discussion, the adsorption rate constant k_{ads} of antibody-conjugated gold nanoparticles also depends on the surface coverage, which is related to the orientation and density of the adsorbing proteins, as well as the surface transport of the labels as they attempt to find open binding sites.

Relationship between ODR and Surface Coverage (Γ). In order to fit the kinetic model to the experimental data, we needed to establish the relationship between normalized ODR and the surface coverage with nanoparticles (Γ). Silver enhancement is widely used to detect nanoparticle binding in assays and microscopy,[21−23] yet the correlation between the surface concentration of nanoparticles and the degree of enhancement has not been quantified adequately. In the experimental characterization of this relation, we used microscope glass slides that were uniformly functionalized with amino (NH_2) groups using APTES self-assembly.[45] Negatively charged gold nanoparticles were electrostatically deposited on the glass slide such that their number density varied in a continuous gradient from one end of the substrate to the other.

The density of gold nanoparticles at various positions was determined by AFM prior to the silver enhancement. This allowed correlating the results of the densitometry analysis after enhancement to the particle surface density (Figure 3). Scanning electron microscopy (SEM) micrographs were also taken before and after silver enhancement to observe how selectively the silver metal is deposited on the gold nanoparticles and how significantly it increases their size (Figure 4). The SEM was performed on a silicon wafer (instead of glass) in order to improve the resolution of the images.

The ODR data in Figure 3 increased approximately linearly for nanoparticle densities below 1.5×10^{10} particles cm^{-2} and then gradually leveled off. The dispersion in the data in regions a and b could result from difficult to control effects on the rate of silver nucleation for experiments performed on different days such as slight variations in the temperature, degree of premixing of the solutions and others. As we estimate the packing density of gold nanoparticles in the sandwich immunoassays to be to be $\sim 10^{10}$ particles cm^{-2}, we assume that ODR increases linearly with Γ and eq 7 can be rewritten as

$$\Gamma/\Gamma_{max} = ODR/ODR_{max} = 1 - \exp(-k_{ads} c_b t) \qquad (8)$$

This simplified adsorption rate eq 8 was used for modeling all of our experimental data. The time constant of this equation is defined as $\tau = 1/k_{ads} c_b$ (s). Like most other first-order linear time-invariant systems, the signal was assumed to reach saturation at the end of 3τ, which corresponds to 95% of the ODR_{max} value.

Assay Sensitivity: Effect of Major Parameters. Typical optical images of two silver-enhanced immunoassay spots for sandwich assays are shown in Figure 2b and c. The optical darkness depends both on the concentration of the reagents used and on their time of incubation. For example, spot b, which appears darker than spot c, was obtained by conducting the experiment with a higher concentration of antigens but for a smaller incubation time of gold suspension than (c). Both spots appear slightly darker at the periphery because of the higher concentration of antibodies due to evaporation-driven convective transport within the droplet during the surface immobilization process. This phenomenon is known as the "doughnut effect" in biological systems[46] (or the "coffee stain effect" in colloid science[47,48]) and persisted despite our efforts to minimize evaporation. To determine the sensitivity of the assays, the concentration and incubation time of antigens and antibody-conjugated nanoparticles were varied systematically.

(i) Effect of Antigen Concentration and Incubation Time. In one series of experiments, we incubated different concentrations of the analyte mouse IgG for a fixed time in order to determine the minimum concentration of antigens required to

(41) Oberholzer, M. R.; Stankovich, J. M.; Carnie, S. L.; Chan, D. Y. C.; Lenhoff, A. M. *J. Colloid Interface Sci.* **1997**, *194*, 138−153.
(42) Shriver-Lake, L. C.; Donner, B.; Edelstein, R.; Breslin, K.; Bhatia, S. K.; Ligler, F. S. *Biosen. Bioelectron.* **1997**, *12*, 1101−1106.
(43) Surovtsev, I. V.; Razumov, I. A.; Nekrasov, V. M.; Shvalov, A. N.; Soini, J. T.; Maltsev, V. P.; Petrov, A. K.; Loktev, V. B.; Chernyshev, A. V. *J. Theor. Biol.* **2000**, *206*, 407−417.
(44) Karlsson, R.; Michaelsson, A.; Mattsson, L. *J. Immunol. Methods* **1991**, *145*, 229−240.
(45) Bhat, R. R.; Fischer, D. A.; Genzer, J. *Langmuir* **2002**, *18*, 5640−5643.
(46) Blossey, R. *Nat. Mater.* **2003**, *2*, 301−306.
(47) Deegan, R. D.; Bakajin, O.; Dupont, T. F.; Huber, G.; Nagel, S. R.; Witten, T. A. *Nature* **1997**, *389*, 827−829.
(48) Parisse, F.; Allain, C. *Langmuir* **1997**, *13*, 3598−3602.

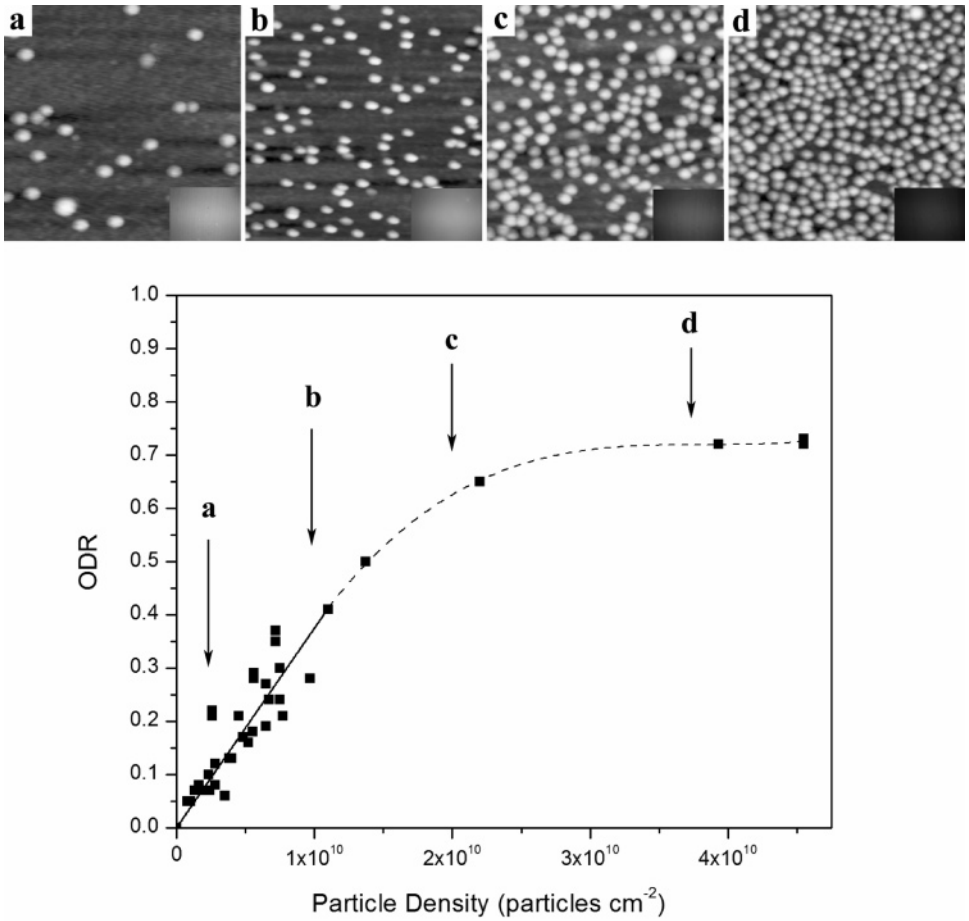

Figure 3. Top: AFM micrographs of varying densities of ~12-nm gold nanoparticles adsorbed on a glass substrate. Optical images corresponding to these particle densities taken after silver enhancement are shown in the insets. Bottom: The graph shows an approximately linear relationship between ODR and gold nanoparticle density at low coverage. The curves are to guide the eye; the densities corresponding to the frames above are labeled with arrows.

saturate the binding receptor sites present on the surface and to obtain a clearly discernible signal. This set of experiments simulates assays where sample concentration or availability is limited, so it is important to minimize the amount of antigen required for detection. In a second set of experiments, we incubated a fixed concentration of mouse IgG (50 μg cm^{-3}) for varying time intervals. The concentration of anti-mouse conjugated gold nanoparticles was held constant at 6.8×10^{13} particles cm^{-3}, and their incubation time was 45 min in all experiments.

One important feature of eq 8 is that the adsorption depends on the product $c_b t$. Thus, we can collapse the data from experiments at varying antigen concentration and varying incubation time on a single master curve. The ODR signals obtained from these two sets of experiments plotted together as a function of the product of antigen concentration and incubation time are shown in Figure 5. The data were fitted with eq 8 by performing a Levenberg−Marquardt nonlinear regression of k_{ads} and ODR_{max} (OriginLab Corp.) until χ^2 error was minimized. An adsorption rate constant of $(1.0 \pm 0.2) \times 10^{-16}$ cm^3 molecules^{-1} s^{-1} was estimated by the model, which compares well with values reported in the literature.[34,40,43,44] The results prove that the experimental data acquired independently by varying the antigen concentrations and incubation times collapse to a single master curve, which, as explained further down, can be a powerful tool in assay optimization.

The scatter in the experimental data in Figure 5 was likely due to the nonuniform darkness of the spots at the edges due to coffee ring effects or drying of the immunoglobulins on the surface. This effect is hard to quantify during the densitometry analysis. More uniform spots may be attained by controlling the humidity in the chamber, performing the assay on a hydrophobic substrate, or convective speeding up of the adsorption process.[18] Additionally, the silver enhancement procedure is complex and the response may become nonlinear if the adsorption of the nanoparticles is uneven and too high. The analysis of the data in Figure 5 shows that the ODR signal saturated at 3.75 μg cm^{-3} (at the end of 3τ). The minimum concentration of mouse IgG detected in 20-min incubation time was 0.1 μg cm^{-3} (0.67 nM). The ODRs of the silver-enhanced spots below this concentration were <0.001 so 0.1 μg cm^{-3} was assumed to be the lowest limit of detection (LOD) of the immunoassay. The sensitivity limit lies within the range of a typical natural immune response in a human body[49,50] and also compares well with some previously reported silver-enhanced and alternative assay techniques.[9,12,33,51] Some authors

(49) Anthony, B. F.; Concepcion, I. E.; Concepcion, N. F.; Vadheim, C. M.; Tiwari, J. *J. Infect. Dis.* **1994**, *170*, 717−720.
(50) Granoff, D. M.; Shackelford, P. G.; Suarez, B. K.; Nahm, M. H.; Cates, K. L.; Murphy, T. V.; Karasic, R.; Osterholm, M. T.; Pandey, J. P.; Daum, R. S. *N. Engl. J. Med.* **1986**, *315*, 1584−1590.
(51) Quinn, C. P.; et al. *Emerg. Infect. Dis.* **2002**, *8*, 1103−1110.

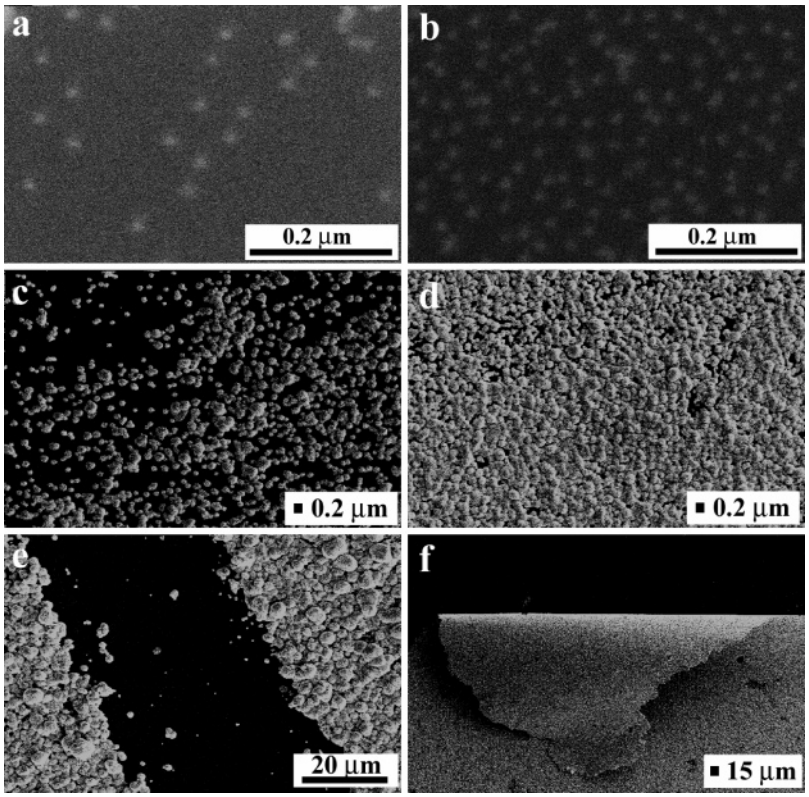

Figure 4. SEM images of samples containing ~12-nm gold particles deposited on an APTES-functionalized silicon wafer. (a, c) Areas of low coverage before and after silver enhancement. (b, d) Areas of high coverage before and after silver enhancement. (e, f) Silver layer deposits imaged at high and low magnification.

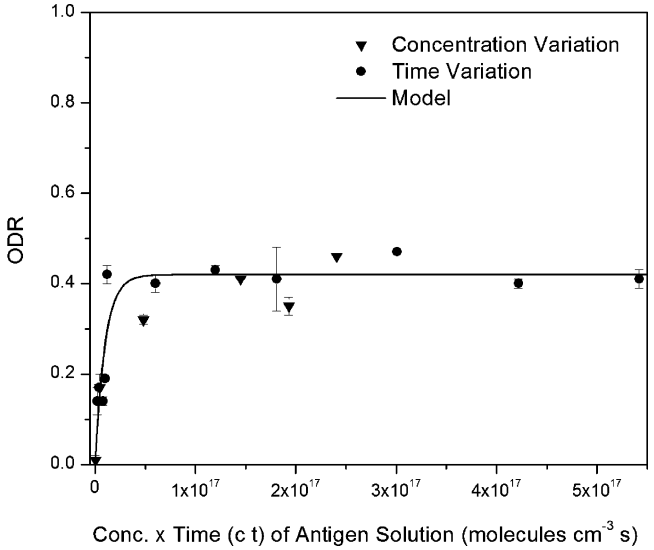

Figure 5. Optical darkness of silver-enhanced spots as a function of the product of antigen concentration in solution and incubation time (*ct*). (▼) various concentrations of mouse IgG antigen incubated for 20 min each and (●) 50 μg cm^{-3} mouse IgG solution incubated for varying time intervals. The concentration and incubation time of gold nanoparticle suspension were 6.8 $\times$ 10^{13} particles cm^{-3} and 45 min in every experiment. The adsorption rate constant of the fitted curve is (1.0 $\pm$ 0.2) $\times$ 10^{-16} cm^3 molecules^{-1} s^{-1}.

report silver-enhanced assays for analyzing antibodies,[29] proteins,[52] viruses,[53] and DNA[28,54] that have a lower LOD, but our method offers miniaturization and the total amount of sample used in the process is very small (<4 ng total).

One key advantage of using silver enhancement detection is that we obtain a high-intensity signal within the first few minutes of antigen incubation. The kinetic data in Figure 5 indicate that the signal intensity was saturated even before the first reading was recorded, i.e., within 1 min of incubation with antigens. This strong rapid response of the immunoassay, visible to the naked eye, could be useful for many diagnostic applications where a rapid yes/no type detection is desired.

(ii) Effect of Concentration and Incubation Time of Gold Nanoparticle Suspension. The bound antigens in the colloidal sandwich immunoassay were detected by binding with antibody-conjugated gold nanoparticles. The diffusion rates of the nanoparticle labels are smaller than that of the free antibody. The antibody-conjugated particle binding could be the time-limiting step in the assay unless a high concentration of nanoparticles is used. The gold nanoparticle conjugates are, however, expensive and their excessive use increases the overall cost of the immunoassay. To determine the minimum concentration of gold nanoparticles required for generating a clearly detectable signal within a certain amount of time, we incubated different concentrations of the gold nanoparticle suspensions for a fixed time and collected the ODR data (Figure 6). The concentration and incubation time of the analyte mouse IgG was 50 μg cm^{-3} and 20 min, respectively, in every experiment. In a related experiment,

(52) Wang, Z.; Lee, J.; Cossins, A. R.; Brust, M. *Anal. Chem.* **2005**, *77*, 5770−5774.

(53) Liu, H.-H.; Cao, X.; Yang, Y.; Liu, M.-G.; Wang, Y.-F. *J. Biochem. Mol. Biol.* **2006**, *39*, 247−252.

(54) Li, B.-S.; Zhao, L.-F.; Zhang, C.; Hei, X.-H.; Li, F.; Li, X.-B.; Shen, J.; Li., Y.-Y.; Huang, Q.; Xu, S.-Q. *Anal. Sci.* **2006**, *22*, 1367−1370.

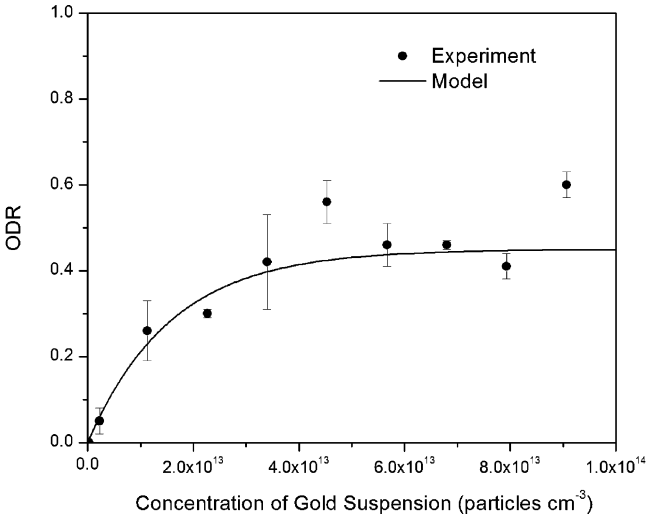

Figure 6. Optical darkness of silver-enhanced spots vs concentration of gold nanoparticle suspension incubated for 45 min. The concentration and incubation time of M IgG antigens were 50 μg cm^{-3} and 20 min in every experiment. The adsorption rate constant of the fitted curve is (2.4 ± 0.6) × 10^{-17} cm^3 molecules^{-1} s^{-1}.

we held the concentration of the gold suspension fixed at 6.8 × 10^{13} particles cm^{-3} and incubated it for different periods of time. These experiments were performed with four mouse IgG concentrations: 50, 30, 20, and 5 μg cm^{-3} (Figure 7) incubated for 20 min in every experiment.

The experimental data in Figure 6 and 7 could not be fitted globally with a single adsorption rate constant. The results of the fitting procedure indicated that the concentration of the antigens on the surface strongly modulated the kinetics of capture of the nanoparticle conjugates in suspension, such that the gold nanoparticles were adsorbed much faster at low antigen concentrations as compared to high ones. It was possible to fit the kinetic data collected for 5−30 μg cm^{-3} mouse IgG concentrations (Figure 7b−d) using a single rate constant, the value of which was estimated to be k_{ads} = (2.2 ± 0.5) × 10^{-16} cm^3 molecules^{-1} s^{-1} by the model. The ODR$_{max}$ values increased proportionally with the antigen concentrations. The kinetic data for 50 μg cm^{-3} mouse IgG concentration (Figures 6 and 7a), however, yielded a much smaller rate constant, k_{ads} = (2.4 ± 0.6) × 10^{-17} cm^3 molecules^{-1} s^{-1}.

The data fitting results suggest that when the analyte concentration is low (below 30 μg cm^{-3}), resulting in a small number of antigen receptors on the surface, the adsorption rate constant of antibody-conjugated nanoparticles is comparable to that of the antigens (see Figure 5). When the analyte concentration is increased to 50 μg cm^{-3}, so that the antigen receptors form a denser layer on the surface, the rate constant of the nanoparticle conjugates decreases by almost 1 order of magnitude. We hypothesize that the rate of adsorption gets reduced because of steric hindrance between the very densely packed binding sites on the antigen receptors. This causes the adsorbing antibody-conjugated gold nanoparticles to reorient themselves or diffuse laterally in order to reach an available binding site and attain a favorable position. These effects may contribute significantly to longer adsorption times. Analogous two-dimensional steric effects, which slow down the rate of or prevent adsorption at high coverage, have been reported in the literature previously.[55,56]

In Figure 6, the bulk concentration of gold nanoparticles for which the surface reached saturation was 4.5 × 10^{13} particles cm^{-3} and no signal was registered below a concentration of 2 × 10^{12} particles cm^{-3} (3.32 nM). The dispersion of the data at higher concentrations of gold nanoparticles increased dramatically (Figure 6). This may again be attributed to variation and uneven packing of the particles at high surface coverage that can lead to a nonlinear increase in silver enhancement and as a result to a high scattering in the ODR signal. The receptor sites for 30 μg cm^{-3} mouse IgG concentration saturated within 5 min, whereas the time required was ~30 min for 50 μg cm^{-3}. The metal spots, however, were lighter (albeit clearly distinguishable by the naked eye) in the former case. The rapid increase in metal surface coverage with time for silver-enhanced immunoassays developed with 30 μg cm^{-3} mouse IgG is shown in Figure 8.

Formulation of General Procedure for Assay Optimization. Development of assays similar to the one studied here is commonly done by empirical optimization until a protocol achieving the desired sensitivity and selectivity is formulated. These protocols include relatively long times for incubation and adsorption of the antigens and labels. Few studies have ever considered the exact time required for achieving the desired degree of surface coverage in each incubation step. The model that we have developed and tested here could allow formulation of such a procedure. We have determined the minimum incubation times required to reach saturation (95% of the ODR$_{max}$ value at the end of 3τ) for several concentrations of antigens and antibody-conjugated nanoparticles (see Table 3). The analysis of these results allows us to design a general algorithm to minimize the incubation time for a narrow range of analyte concentrations. This algorithm applies to any antibody−analyte binding that follows adsorption-limited kinetics similar to our assay system. It makes use of our finding that the adsorption is proportional to the product of the incubation time and analyte concentration; thus, this product will remain constant at the optimal adsorption. Once the optimal time for one analyte or label concentration is determined, the smallest time for lower or higher concentrations could be established by the relation $t_1c_1 = c_2t_2$, or the smallest label concentration for a certain target incubation time can be calculated. The data reported in Table 3 confirm that the product of the incubation time and analyte concentration (c_bt) always remains constant for both the analyte and gold labels. In addition to Table 3, Figure 6 also proves that the product c_bt is a suitable parameter group for collapsing the change in the optical signal on a single master curve.

We propose a procedure for assay optimization that could operate as follows: First, an analyte or label of known concentration (c_1) is incubated for different periods of time while all other parameters are held constant. Second, the ODR values of the developed silver-enhanced spots are measured and plotted as a function of time. Third, the experimental data are fitted with the adsorption-limited rate eq 8 by varying k_{ads} and ODR$_{max}$ parameters until the least χ^2 error between the data and the model is minimized. Fourth, the value of time constant ($\tau = 1/k_{ads}c_1$) is

(55) Schaaf, P.; Talbot, J. *J. Chem. Phys.* **1989**, *91*, 4401−4409.
(56) Sips, R. *J. Chem. Phys.* **1948**, *16*, 490−495.

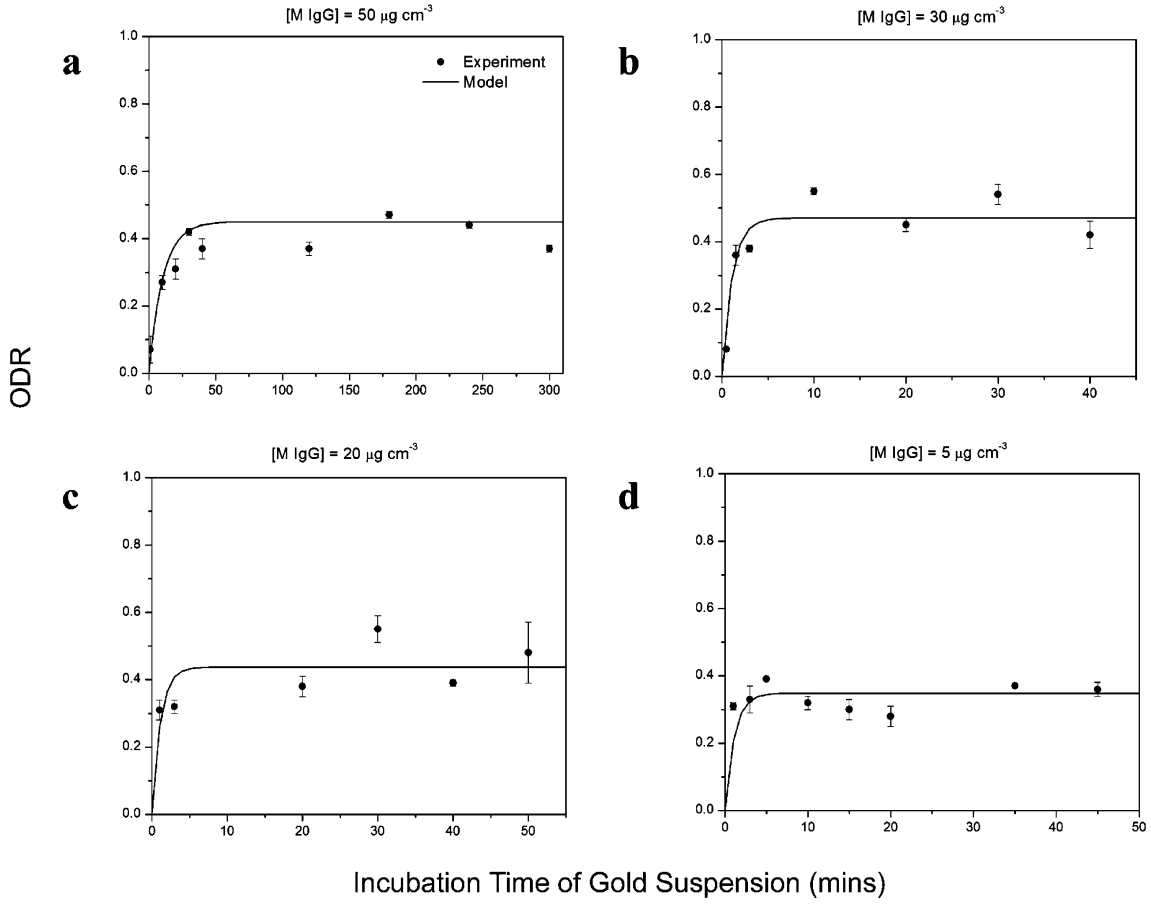

Figure 7. Optical darkness of silver-enhanced spots vs incubation time of 6.8×10^{13} particles cm^{-3} concentrated gold nanoparticle suspension. The plots are for different concentrations of M IgG antigens: (a) 50, (b) 30, (c) 20, and (d) 5 μg cm^{-3}. The incubation time of antigens was 20 min in every experiment. The adsorption rate constants of the fitted curves are as follows: (a) $(2.4 \pm 0.6) \times 10^{-17}$ and (b−d) $(2.2 \pm 0.5) \times 10^{-16}$ cm^3 $molecules^{-1}$ s^{-1}.

determined for the assay process and a certain criterion for completeness is established (e.g., $t_1 = 3\tau$, where 95% of adsorption will be complete). Finally, the relation $3\tau c_1 = c_2 t_2$ is used to calculate the smallest incubation time (t_2) for any other known concentration (c_2) of the same solute or to estimate the required label concentration for a target incubation time t_2.

CONCLUSIONS

We characterized the performance of a compact and low-cost nanoparticle sandwich immunoassay and proposed a general semiquantitative scheme to optimize its overall performance using a mass-transfer model. The results point out that the mass transfer of the antigens and gold nanoparticle labels in the immunoassay was controlled by the rate of their adsorption at the surface. A carefully designed experiment proved that the opacity of the silver-enhanced spots increased linearly with the surface density of gold nanoparticles. A simple kinetic rate equation was used to fit all our data. The binding rate constant of antibody-conjugated gold nanoparticles was a function of the density of the antigen receptors on the surface. It was 1 order of magnitude higher for low coverages. The selectivity achieved with our immunoassay was adequate in the sandwich format although false positives occurred in direct assays. The lower limit of antigen detection of this method was 0.1 μg cm^{-3} (total of 4 ng of antigen). This LOD value

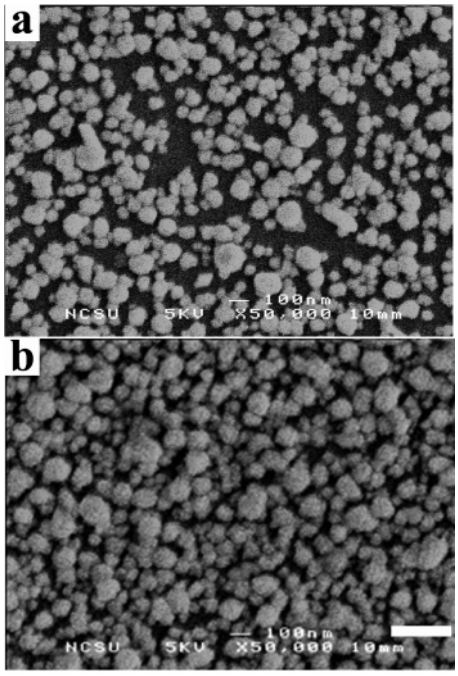

Figure 8. SEM images of silver-enhanced immunoassays after (a) 1.5 and (b) 10 min of incubation with gold nanoparticle suspension. The concentration and incubation time of M IgG antigens were 30 μg cm^{-3} and 20 min in both experiments. The scale bar represents 30 μm.

Table 3. Smallest Incubation Times Required To Reach Saturation for Different Concentrations of Analyte and Nanoparticle Conjugates

	mouse IgGs			goat anti-mouse IgGs conjugated to gold particles		
type of solution	concn c_b (μg cm^{-3})	incubation tme t (min)	product $c_b t$	concn c_b (particles cm^{-3})	incubation time t (min)	product $c_b t$
I	50	1.5	75	4.5×10^{13}	45	2.02×10^{15}
II	3.75	20	75	6.8×10^{13}	30	2.04×10^{15}

is not extraordinarily high but is comparable to some of other state-of-the-art detection techniques. The developed immunoassays produce a signal that can be visualized by naked eye. The silver-enhanced plates also have the advantage of being stable and portable. More importantly, these immunoassays could be key in future on-chip microarrays and microassays thanks to their high potential for miniaturization and easy interfacing with electronic circuits. The nanoparticle labeling may be performed between a pair of electrodes, which will be short-circuited by the metallic silver, only if a specific analyte is detected in the sample solution.[30−32] Outcomes of biospecific interactions could then be monitored directly by electrical measurements in real time. The electric readout could allow parallel processing of a series of immunoassays on a single chip, each of which can be miniaturized below the size restrictions of conventional optical detection.

ACKNOWLEDGMENT

This study was supported by grants from the National Science Foundation (NSF) and the U.S. Army Research Office (ARO). We are grateful to Rajendra Bhat for APTES gold gradients, Jeong-Seok Na and Greg Parsons for AFM measurements, and Brian Prevo for assistance with the SEM observations.

Received for review December 11, 2006. Accepted March 18, 2007.

AC062341M